Torsional modal analysis made easy – Methodology and practical examples from electric motor testing

T. Kimpián [1], F. Augusztinovicz [2]
[1] thyssenkrupp Components Technology Hungary Ltd.
Budafoki way 56., H-1117, Budapest, Hungary
e-mail: **tibor.kimpian@thyssenkrupp-automotive.com**

[2] Budapest University of Technology and Economics, Department of Telecommunications
Magyar Tudósok körútja 2., H-1117, Budapest, Hungary

Abstract
In this paper we present a very efficient torsional modal analysis method that utilizes the tested permanent magnet synchronous motor as a broadband torsional vibration exciter and we show how to utilize standard accelerometers in order to measure small amplitude torsional vibration and how to obtain the necessary FRFs for torsional modal analysis. After introducing the basic concepts and presenting the test setup, the generation of any cylindrical object's wire-frame geometry, the animation of torsional mode shapes, results from two different motor testbenches are also shown. One uses a standard industrial asynchronous motor as a load machine, while in the other configuration a hysteresis brake is providing the necessary breaking torque during the measurement.

1 Introduction

Electrification of passenger and transport vehicles is a ubiquitous trend nowadays, that concerns not only the traction drive system but the auxiliary and comfort systems as well. Due to the lack of the continuous power consumption of the hydraulic pump and outstanding versatility as an actuator, Electric Power Assisted Steering (EPAS) systems are now widely used in almost all vehicle sectors. Of course, as for the main drive systems, high power density, low weight and cost efficiency are key requirements for the EPAS as well, and the aforementioned requirements are typically fulfilled by utilizing Permanent Magnet Synchronous Motors (PMSMs) [1].

NVH analysis of these complex mechatronic systems reveals that beside the vibration of the rotor and stator system, the torque fluctuation is also a major contributor to the perceived tonal noise, therefore precise measurement of sub Ncm torque-ripple is necessary during motor NVH testing.

Due to the fact that a steering system operates over a very wide speed range, the above accurate broadband measurement of torque-ripple of steering motors is an everyday task in the development. Experience shows, that the modal behavior of the test equipment has significant influence on the measured torque-ripple, therefore determining the torsional mode shapes of the test assembly including the tested motor is an important step in test equipment development.

In the next section we are going to briefly outline the motivation behind the development of an easy to use torsional modal analysis methodology utilizing some remarkable properties of permanent magnet synchronous motors.

2 Motivation

The primary motivation of the work is to better understand the behavior of test equipment that is used for NVH testing of PMSMs (Figure 1). The test setup contains (from left to right) 1.: asynchronous load motor, 2.: coupling between the load motor and the torque sensor, 3.: torque sensor, 4.: non-contact optical incremental encoder, 5.: coupling between the torque sensor and the EPS motor, 6.: tested EPS motor, 7.: 3D coordinate table for shaft alignment and 8.: triaxial and single axis accelerometers.

The dynamic behavior of the fixation (3D coordinate table) and the tested motor (EPS motor) can be easily measured and/or simulated by traditional Experimental Modal Analysis (EMA) and/or FEM methods and therefore it is clearly understood and its effect in the acceleration response measured by a standard triaxial accelerometer can be taken into account easily. However measuring the dynamic torque response of this test setup only using standard NVH equipment requires special methods outlined in this article.

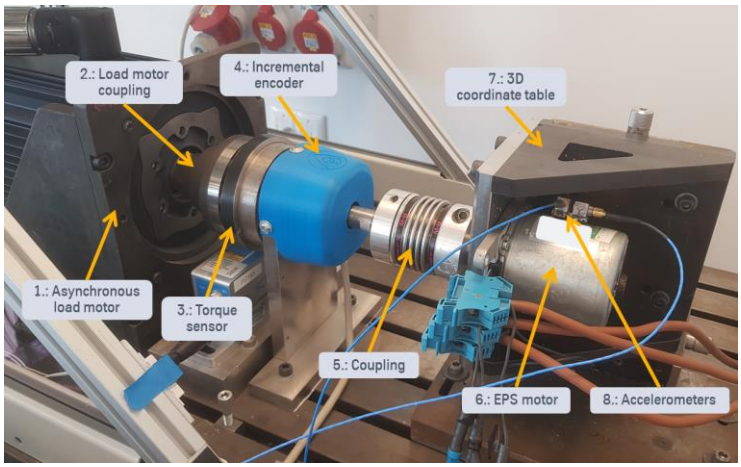

Figure 1: Typical test setup for EPAS motor NVH testing on Testbench Nr.1.

Figure 2 shows Campbell diagram evaluation of the torque signal in CW and CCW turning direction of a typical 30 s long linear run-up measurement of a 9 slot 6 pole PMSM that is readily used in low to medium power column type power assisted steering systems. It is clearly visible, that the torque ripple of the motor is significantly amplified by torsional resonances at 547 Hz, 725 Hz and 1046 Hz in both turning directions.

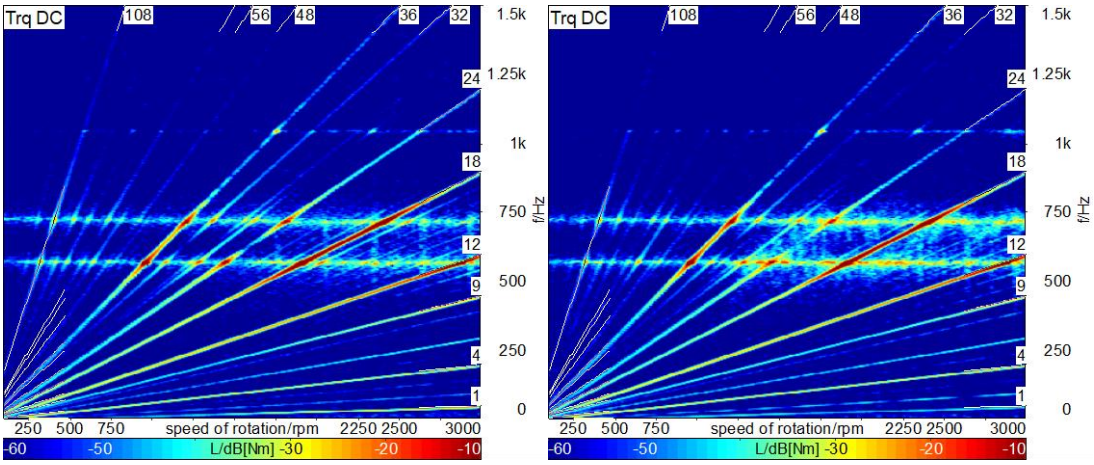

Figure 2: Typical Campbell diagrams of the torque signal of a 30 s long linear run-up measurement of a 9/6 PMSM from testbench Nr. 1. The left picture shows CW (ClockWise) while the right picture shows CCW (CounterClockWise) turning direction respectively. The resonances at 574 Hz, 725 Hz and 1046 Hz are well visible and they are significantly influencing the dynamic torque measurement.

The 18th (left side) and 36th (right side) order torque ripple evaluated in both turning direction (1.: CW, 2.: CCW) can be seen on figure 3. The effect of the three resonances is clearly visible. In order to properly understand where those resonances come from a simple and straight forward torsional modal analysis method is proposed in this article.

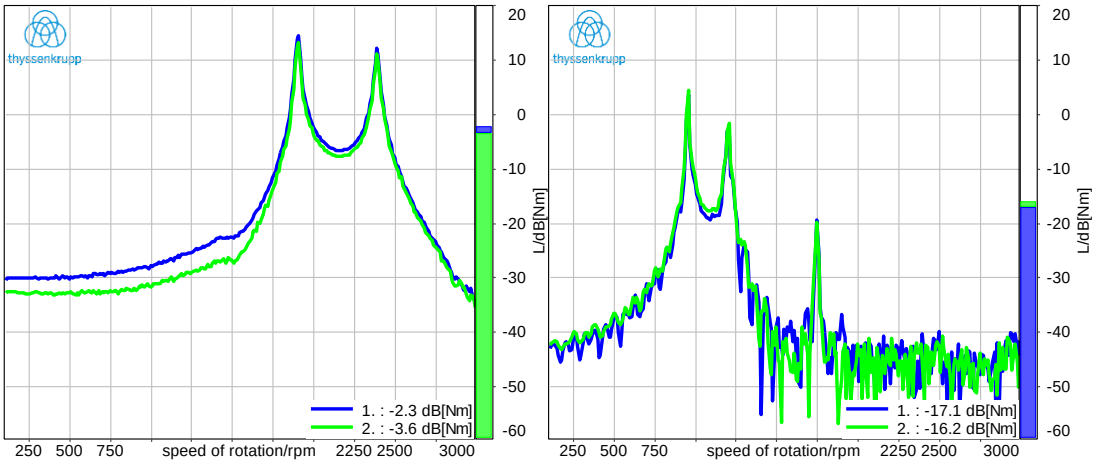

Figure 3: 18th (left side) and 36th (right side) order torque ripple of the tested 9/6 EPS motor at full load in CW (1.) and CCW (2.) direction.

First, the analogy between rectilinear and torsional dynamic systems is shown and after that the torsional vibration excitation method is introduced. The specialty of the proposed method is, that the tested EPAS motor is used as an electrodynamic torsional shaker in order to excite the system with small amplitude torsional vibration, hence the shaft system is not turning and therefore the angular acceleration can be measured using traditional accelerometers. The estimation of the measured transfer functions was done using the well-known Rational Fractional Polynomial (RFP) method and a custom geometry visualization and animation program has been written in MATLAB in order to evaluate the results.

After going through step-by-step the most important items of the proposed method, experimental results are shown from two different motor NVH testbenches. The measurement shafts and the load machines are different between the two setups, therefore one goal of the investigation was to understand the effect of those differences on the measured dynamic torque signal.

3 Description of the proposed torsional modal analysis method

The off-the-shelf available software solutions typically support the entire EMA process from sensor calibration, excitation signal generation for shaker testing (however, that is limited to standard excitation signals), data acquisition, curve fitting, preparation of geometry, animation of mode shapes, correlation to FEM data, etc. For rectilinear systems the excitation methods are rather standard either using an impact hammer or by means of electrodynamic shaker(s), and the responses are typically measured with piezo broadband accelerometers or laser Doppler vibrometer(s) [2].

In torsional systems the dynamic excitation is typically provided by one or more component of the rotating system, therefore most of the time Operational Deflection Shapes (ODS) can be determined or Operational Modal Analysis (OMA) may be carried out. Measuring torsional vibration is typically done by optically or magnetically measuring the rotational speed of various components and by means of FM demodulation the torsional vibration signal can be obtained. The obtained torsional vibration data can be used for further analysis just like any traditional vibration signal measured by e.g. an accelerometer.

According to the authors knowledge standard rotational vibration exciters are not available on the market, therefore each application requires custom solutions for torsional vibration excitation like for example the one proposed by C. Sihler in [3].

3.1 Analogy between rectilinear and torsional mechanical systems

As table 1 shows, by choosing the appropriate quantities, rectilinear and torsional mechanical systems behave exactly the same way as they are completely analog to each-other, therefore the standard EMA methods developed for rectilinear systems can be used for torsional systems as well [4]. This article tries to give ideas how to obtain the necessary transfer functions for EMA using only off-the-shelf available equipment in a perhaps unusual way to accomplish the above task.

Table 1: Analogy between rectilinear and torsional mechanical systems

Physical quantity	Rectilinear vibration		Torsional vibration	
	Symbol	Unit	Symbol	Unit
Time	t	s	t	s
Displacement	x	m	φ	rad
Velocity	$\dot{x}$, v	m/s	$\dot{\varphi}$, ϑ	rad/s
Acceleration	$\ddot{x}$, a	m/s^2	$\ddot{\varphi}$, β	rad/s^2
Force / Torque	F	N	M	Nm
Mass / Inertia	m	kg	J	Nms^2/rad
Spring	k	N/m	K	Nm/rad
Damper	c	Ns/m	C	Nms/rad
Equation of motion	$m\ddot{x}+c\dot{x}+kx=F$		$J\ddot{\varphi}+C\dot{\varphi}+K\varphi=M$	
Natural frequency	$\omega_0=\sqrt{\frac{k}{m}}$	rad/sec	$\omega_0=\sqrt{\frac{K}{J}}$	rad/sec
Damping factor	ξ	dimensionless	ξ	dimensionless

3.2 Excitation method

In order to utilize the tested three phase PMSM as a broadband vibration exciter in principal any broadband signal can be used, however it might be troublesome to drive an impedance as low as 20 – 50 mΩ and 50 – 150 µH using traditional audio and/or shaker amplifiers. It is of course possible to use a high power 4 – 8 Ω resistor in series with the motor's winding in order to avoid the amplifiers protection circuits to limit the output current hence introducing significant distortion [5]. Another issue as shown in previous work is, that in case of single phase drive, the amplitude of the torque excitation depends on the actual rotor position as the coupling between one phase and the rotor is inherently rotor position dependent [6].

In order to overcome the above difficulties multiphase multisine phase currents provide the best excitation, as it can be shown that rotor position independent amplitude broadband torque can be obtained using appropriate excitation conditions [7]. For ideal drive conditions a special current output amplifier has been designed and used for the measurements. So far only one channel is fully operational of the dedicated test amplifier, but after the completion of the second channel and thorough testing, the amplifier design is also going to be published.

As shown in the next section, the excitation signal has been generated in MATLAB R2020a and played through a MAYA44USB+ audio interface [8] and amplified by the dedicated power amplifier. The phase current of the motor was measured with a HX 05-NP broadband active compensation type current transducer by LEM [9].

3.2.1 Excitation signal

Figure 4 shows the user interface of a small MATLAB application with which the excitation signal has been generated and figure 5 shows the time and frequency domain representation of the generated Schröder multisine signal respectively.

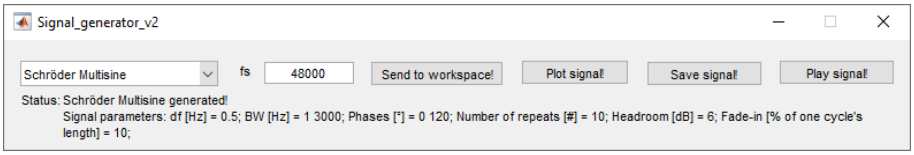

Figure 4: User interface of the signal generator with which the excitation signal has been synthesized.

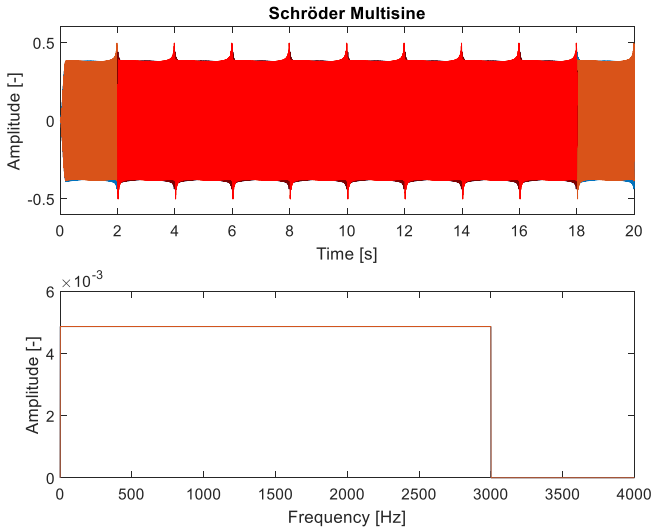

Figure 5: Time and frequency domain representation of the excitation signal. From the 20 s long signal 8 complete periods are selected from the middle in order to showcase how the necessary amount of periods can be selected from the recording during postprocessing.

For generating the signal the following formula has been used [7]:

$$x_i(t) = \sum_{k=1}^{N_k} A_k \cos\left(\omega_k t + \frac{-k(k-1)\pi}{N_k} + \frac{2\pi(i-1)}{N_{ph}}\right) \tag{1}$$

However the synthesis of the signal is implemented in the frequency domain as suggested in [10].

Based on preliminary experience from run-up testing a frequency span from 1 Hz – 3 kHz and a frequency resolution of 0.5 Hz has been selected. For the FRF calculations 8 complete 2s long periods have been used, but in order for the system to have the appropriate initial condition, one period of the excitation signal has been played in advance, and in order to avoid truncation error and/or glitch one period afterwards.

As shown in [6] if the PMSM is excited only on one phase, than the amplitude of the excitation depends on the steady state rotor positions, therefore while placing the accelerometer from one location to the next care must be taken not to change the rotor position, otherwise the FRFs may have different amplitudes causing the mode shapes to be distorted. If the system has rigid body modes, than it is rather easy to check that the measurements are consistent as all points should move in phase with the same angular displacement. If one or more point(s) is/are moving with larger and/or smaller amplitude, than the corresponding FRF(s) shall be rescaled to compensate the mismatch.

3.3 Measurement of torsional vibration using standard accelerometers

In order to perform torsional modal analysis, angular acceleration has to be measured on the corresponding components of the geometry. Utilizing the fact, that due to the special excitation current only small amplitude torsional vibration is present on the shaft system, standard accelerometers can be used to measure tangential vibration and using geometry data, the necessary angular acceleration can be calculated according to eq. 2, where ω and β are the angular velocity and acceleration, v_{tan} and a_{tan} are the tangential vibration velocity and acceleration respectively. Due to the fact, that standard accelerometers do not sense the acceleration on their surface, the distance from their mounting surface to the sensing element has to be taken into account in r.

$$\omega = \frac{v_{tan}}{r} \longrightarrow \beta = \frac{a_{tan}}{r} \tag{2}$$

Figure 6 shows two examples of such sensor placements. The left side shows the sensor mounted on the Rotor Position Sensor (RPS) magnet, where the influence of the sensor geometry on the measurement radius is almost 45 %. On the right side the sensor is mounted on the coupling of the EPAS motor, where the effect of the sensing distance is > 12 %. In practice, it is easy to account for this error while specifying the geometry, therefore the mode shapes are going to be scaled properly.

In this investigation the data acquisition has been done using a HEADlab multichannel data acquisition front-end from HEAD Acoustics, and the calculated FRFs and coherence functions have been exported to MATLAB readable format from ArtemiS software.

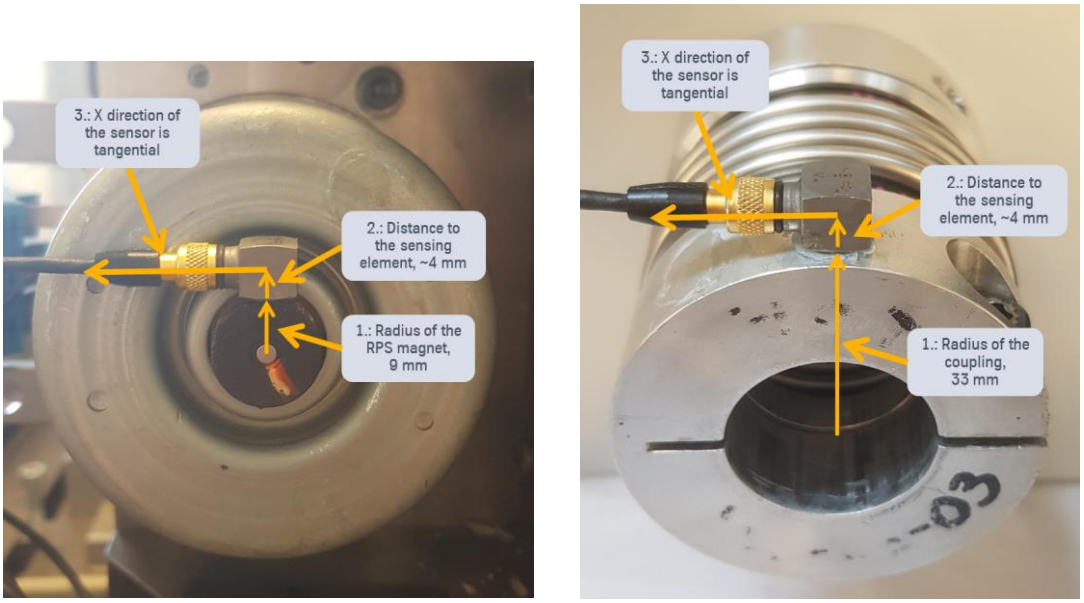

Figure 6: Placement of a small B&K type 4520 triaxial accelerometer on the RPS magnet (left) and on the coupling (right). 1.: radius of the corresponding component, 2.: the distance to the sensing element of the sensor, 3.: direction of the X channel of the sensor, that measures tangential vibration.

3.4 Estimation of the frequency response functions

Seeing the measured transfer functions (figure 13) and considering the fact that only a few modes have to be identified, the Rational Fractional Polynomial (RFP) method has been used for the estimation of the transfer functions. As we will show later, using a frequency domain identification algorithm allows for easy correction of mass loading of the accelerometer, as the mistuned peaks in the individual FRFs can be easily shifted in frequency domain [11], [12].

3.5 Visualization of the geometry and animation of the mode shapes

3.5.1 Visualization of the geometry

In order to properly visualize the torsional mode shapes, a dedicated 3D geometry modeler has been written in MATLAB. As the shaft system of any test equipment basically consists of cylinders, the easiest was to generate the geometry as a series of cylinders in a cylindrical coordinate system. For easy manipulation of the geometry, the circles that the cylinders are consisting of have been drawn on the complex plane. As shown on figure 7 a circle was divided into 16 points (in fact for drawing a complete circle, 17 points have been used), each point represented by a single complex number according to eq. 3.

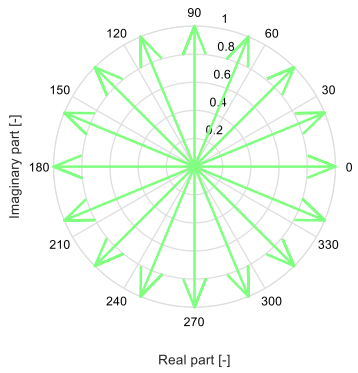

Figure 7: Complex unit vectors representing one circle from the geometry.

$$p_{ik} = r_k e^{j\varphi_i}, \varphi_i = \frac{2\pi\,(i-1)}{N_\varphi} \tag{3}$$

In eq. 3 p_{ik} is the coordinate of the i^{th} point of a circle (where $i = 1 \ldots N_\varphi$) in the geometry of the k^{th} circle. The circles are scaled to the actual radius r_k of the geometry and are repeated along an axis perpendicular to the complex plane. Figure 7 shows the rotor and the first coupling of testbench Nr. 1. as an example. Conversion of the complex vectors from cylindrical coordinate system to Descartes coordinates can easily be done by taking the real and imaginary part of the coordinates and assign them to the corresponding spatial direction. This can happen in the last step before animation, therefore any manipulation of the geometry and the animation can be implemented using complex arithmetic operations.

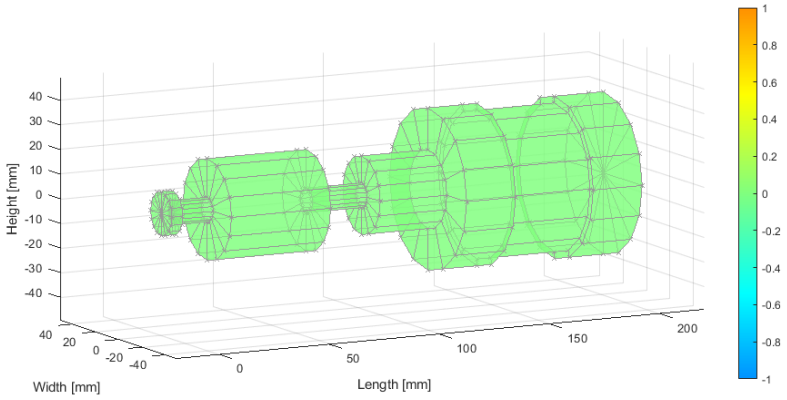

Figure 8: The rotor of the EPS motor and the first coupling from testbench Nr. 1.

3.5.2 Animation of the mode shapes

The animation of the model is achieved by simply multiplying the complex coordinates by an appropriate unit length complex terms (eq. 4), that are containing the mode shape ψ_k on the k^{th} location, the maximum animation amplitude α and the actual angular displacement θ that changes proportionally from $\theta = 0 \dots 2\pi$ in conjunction with the frame index.

$$p_{ik} = r_k e^{j\varphi_i} e^{j\alpha Re\{\psi_k e^{j\theta}\}} = r_k e^{j(\varphi_i + \alpha Re\{\psi_k e^{j\theta}\})} \tag{4}$$

In order to have better visual experience, the coloring of the components is also changed proportionally to the instantaneous angular displacement. A 2D example is given on figure 9, where each of the 16 vectors is moved by ± 4.5°.

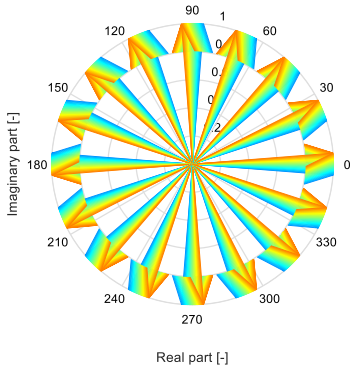

Figure 9: Complex unit vectors showcasing the animation and coloring of the deformed model.

Of course in practice not all the points of the geometry are accessible and/or measurable, therefore it is necessary to map the estimated mode shapes onto the geometry. This is most easily accomplished by an appropriate mapping matrix $\underline{\underline{T}}$ as shown in eq. 5.:

$$\begin{bmatrix} \psi_1 \\ \vdots \\ \psi_K \end{bmatrix} = \underline{\underline{T}} \begin{bmatrix} \psi_1 \\ \vdots \\ \psi_M \end{bmatrix} \tag{5}$$

$\underline{\underline{T}}$ is a binary matrix in most cases and the m^{th} column contains ones in the k^{th} row where the k^{th} point in the geometry is moving according to the m^{th} point of the corresponding mode shape vector. Using elements other than zero and one allow motion to be interpolated for example between two neighboring nodes of a mode shape thus providing more realistic deformations of the geometry.

Figure 10 shows an example how the example geometry from figure 8 can be animated and colored assuming for the example that the inertia of the rotor and the coupling forms a single degree of freedom system with the stiffness of the shaft in between them.

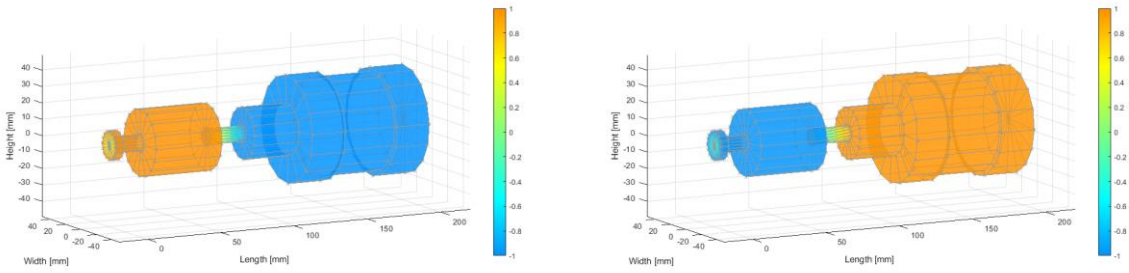

Figure 10: Example animation of the geometry from figure 8.

There are three main advantages of the animation method described. First of all, the generation and animation of any cylindrical object – so in practice any shaft system – can be accomplished with ~100 lines of MATLAB code including saving the animations in *.gif files for presentation. Secondly due to the true vector implementation, during rotation the model does not change its diameter with angular displacement like in many FEM and EMA software packages, but the radius remains constant at all times, hence providing a more realistic animation of torsional phenomena. The third advantage is the true angular displacement coloring, that helps to properly visualize the true relative displacements of the different parts of the assembly which is a very useful feature in practice.

4 Experimental results

In this section we summarize the measurement results for testbench Nr. 1. and 2. and compare them in order to evaluate the influence of the two different braking principles. First the measurement setups are shown including the most important components and the measurement points. Measured FRFs and coherence functions are also presented for each measurement point, after that the average of the fitted transfer functions are shown in their respective frequency range, which is followed by the presentation of identified the mode shapes.

4.1 Mechanical setups and measured FRFs

Figure 11. and 12. shows the measurement points on testbench Nr. 1 & Nr. 2. respectively. The shaft accelerometer was glued on the RPS magnet like shown on figure 6, and the moving accelerometer was moved from point 2 – 10 (2 – 9 for testbench 2.). The FRF for the first point has been taken from the first measurement when the moving accelerometer was on point Nr. 2. After that only the FRF of the moving accelerometer have been added to the FRF set.

As it can be seen on figure 13. the shaft assembly has three major resonances between 500 – 1500 Hz in both setups. Below and above that frequency range a standard second order high-pass and low-pass behavior can be seen respectively. As the phase responses and the coherences indicate, the signal to noise ratio is best in the ~ 500 – 1500 Hz band and as this is the most relevant frequency range from the torque-ripple measurement point of view, these three mode shapes have been analyzed in detail. The phase responses have also been unwrapped in this frequency range, hence the 180° phase shifts are nicely visible at each mode.

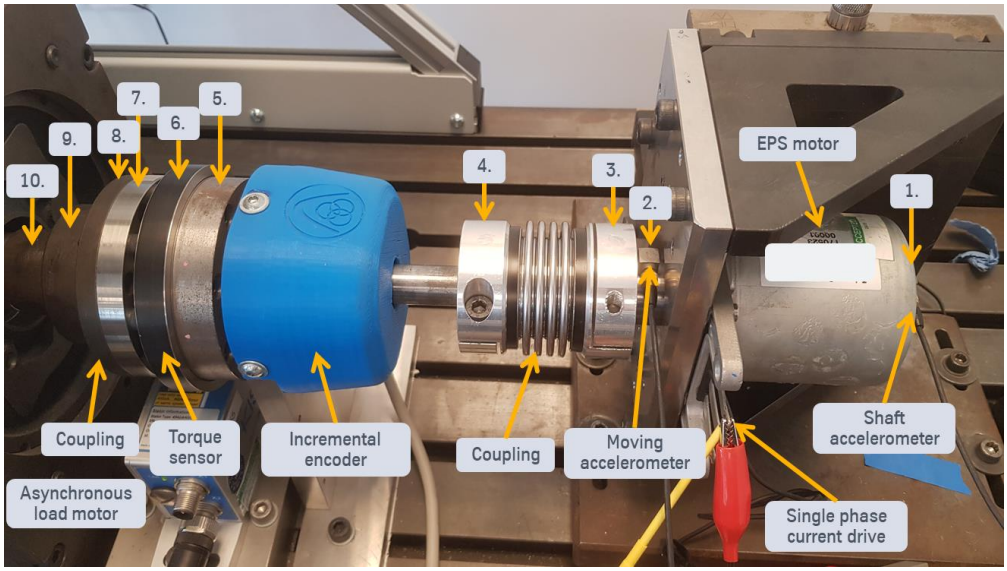

Figure 11: Motor testbench Nr. 1.

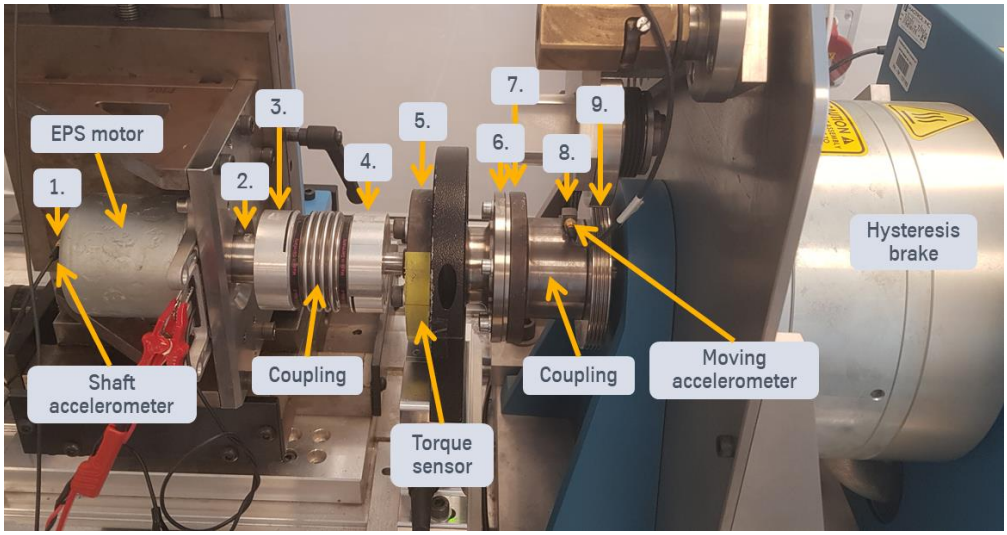

Figure 12: Motor testbench Nr. 2.

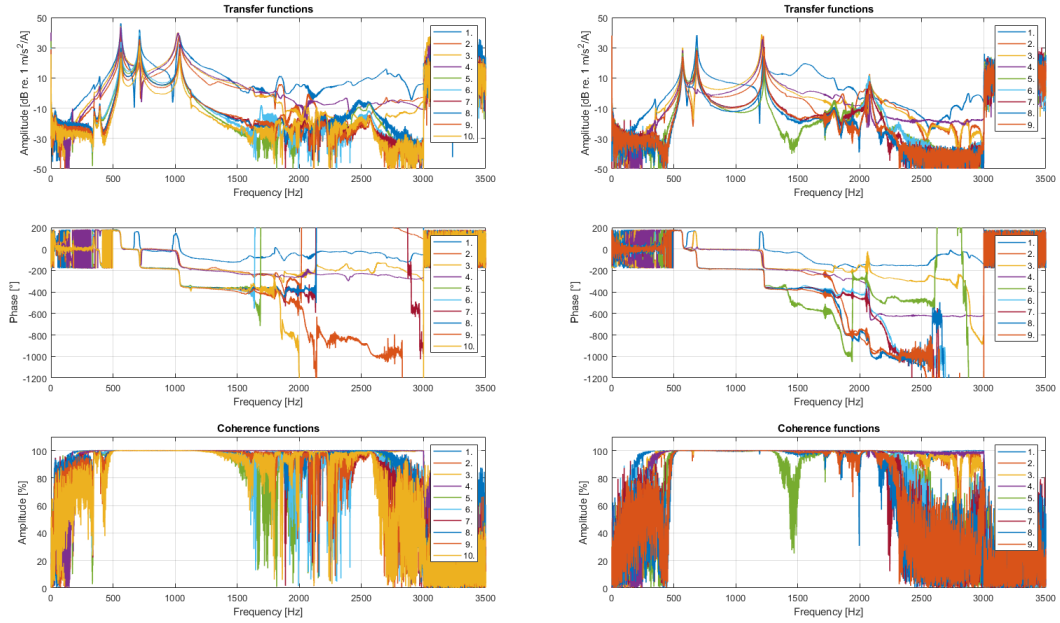

Figure 13: Measured transfer and coherence functions of motor testbench Nr. 1. (left side) and Nr. 2. (right side). The phase responses have been unwrapped between 500 – 1500 Hz hence the 180° phase shifts are nicely visible at the modes.

4.2 Estimated transfer functions and mode shapes

Figure 14 & 15 shows the average of the measured and estimated transfer functions in the 500 – 800 Hz for the first two modes and in the 980 – 1100 Hz & 1100 – 1300 Hz band for the third mode shape respectively. These frequency ranges have been used by the RFP algorithm for FRF estimation with two degree of freedom system models, meaning four zeros and four poles in the nominator and denominator of the estimated transfer functions respectively.

For the third mode the first four FRFs had to be shifted by 4.5 – 14.5 Hz in order to compensate for the mass loading (properly moment of inertia loading) of the accelerometer, as first four points of the third mode shape are the most sensitive to additional inertia.

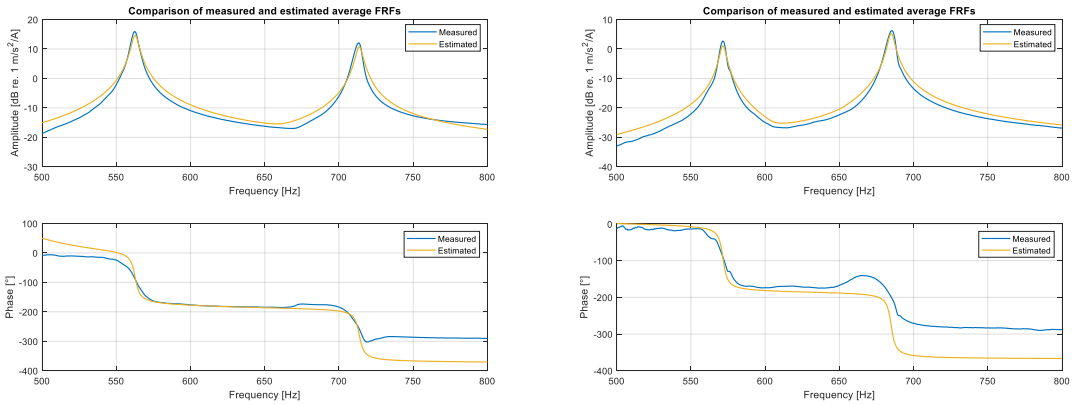

Figure 14: Measured and estimated FRFs for the 1st and 2nd mode of motor testbench Nr. 1. (left side) and Nr. 2. (right side).

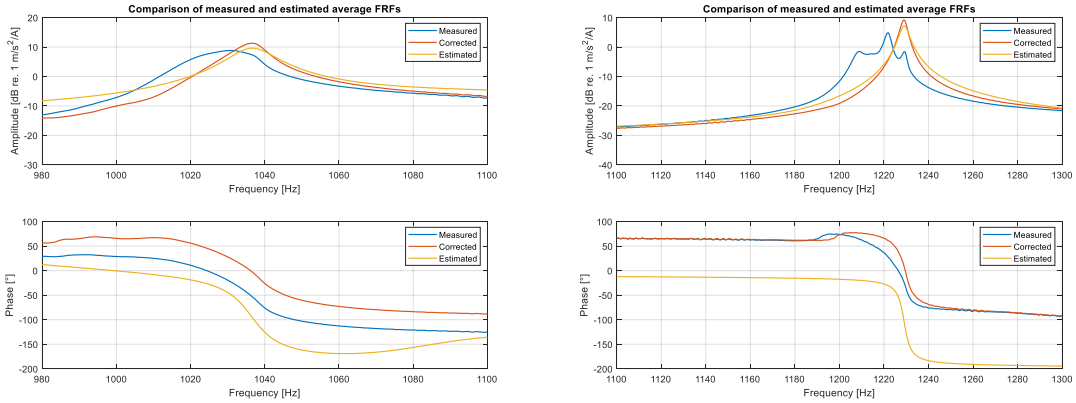

Figure 15: Measured and estimated transfer functions of motor testbench Nr. 2.

Figure 16 – 18 shows the three identified mode shapes represented by their maximum and minimum amplitude state. It might be hard to imagine the motion without animation, however we try to describe each mode shape the best possible way.

The 1st mode (figure 16) is very similar to the 1st mode of a Cantilever beam, where at the fixation point the deflection is zero and monotonically increases until the end of the beam. Here the "fixation point" is the high moment of inertia of the load machine and the free end is the end of the shaft of the EPS motor.

In the 2nd mode shape (figure 17) the rotor of the EPAS motor moves against the torque sensor and the brake coupling. Due to the high difference in inertia, the vibration amplitude of the rotor is significantly higher, therefore the out-of-phase movement of the other half of the resonant system is hardly visible, however in the animation the motion is clearly visible.

Figure 18 shows the 3rd mode shape, where the rotor of the EPAS motor moves against the inertia of the 1st coupling, while the short shaft between the coupling and the torque sensor acts as a torsional spring and mostly isolates the vibration from the torque sensor.

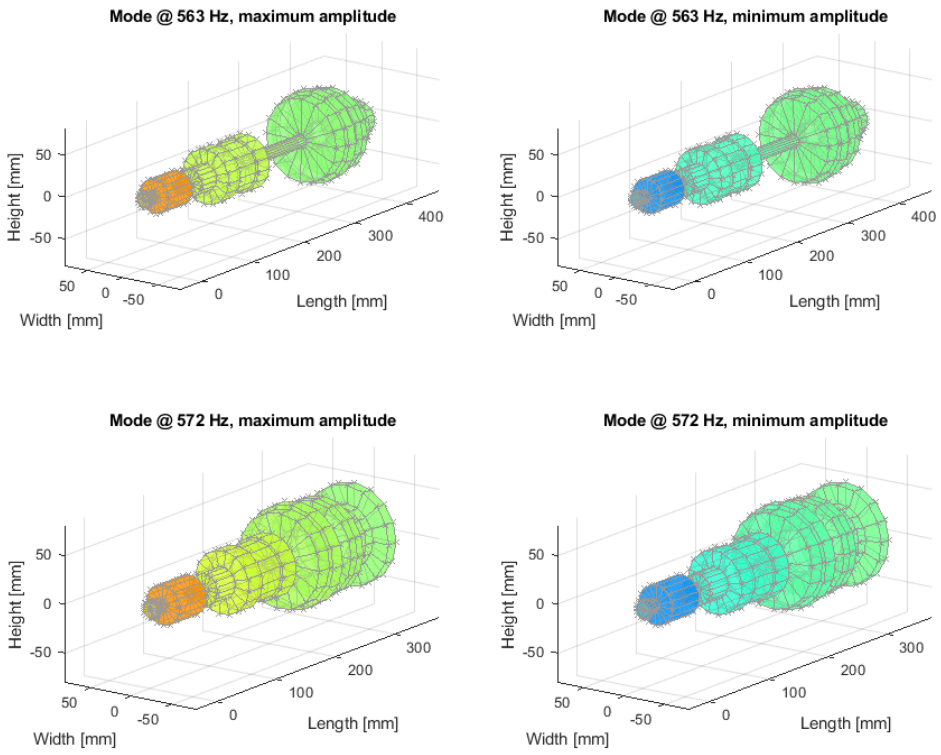

Figure 16: 1st mode of motor testbench Nr. 1 (upper) & Nr. 2. (lower). This mode shape is very similar to the first mode of a Cantilever beam, however here the the EPAS motor has the highest amplitude.

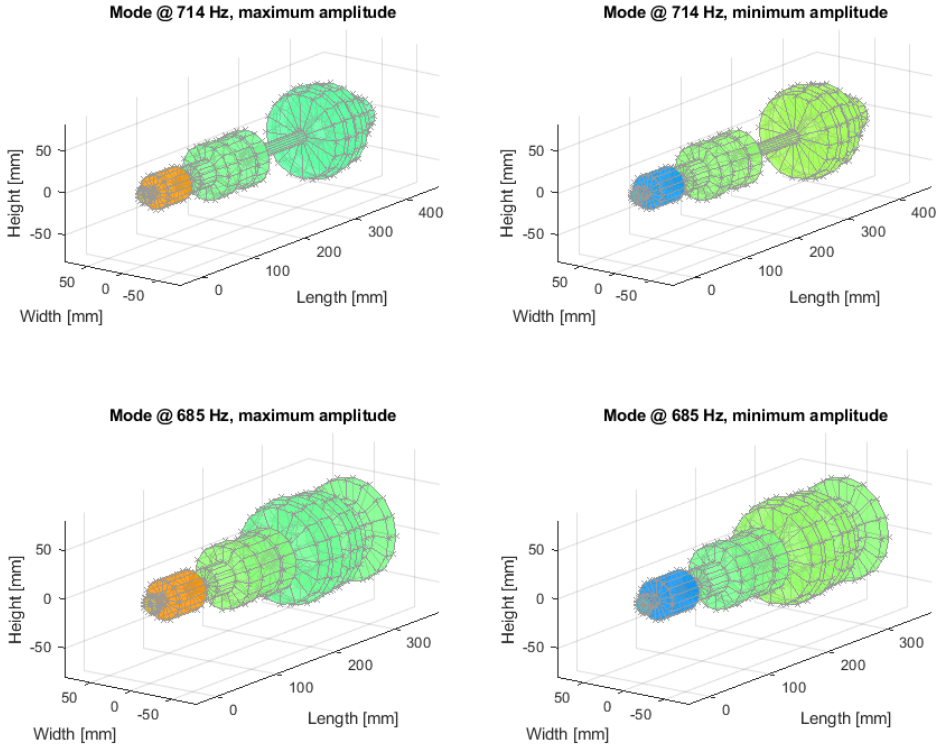

Figure 17: 2nd mode of motor testbench Nr. 1. (upper) & Nr. 2. (lower). In this mode shape the rotor of the EPAS motor and the torque sensor assembly moves against each-other.

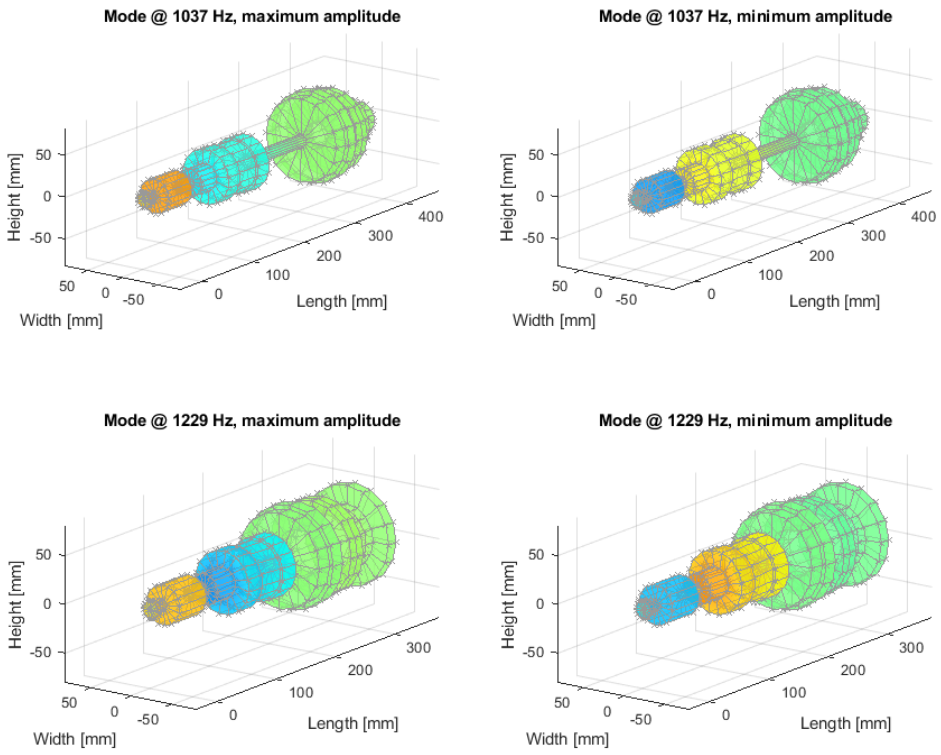

Figure 18: 3rd mode of motor testbench Nr. 1. (upper) & Nr. 2. (lower). In this mode shape the rotor of the EPAS motor is moving against the first coupling and the torque sensor assembly has very low amplitude.

As the measurement of the torque fluctuation is strongly influenced by the above mode shapes, it is important to understand how can the structure and hence these mode shapes be influenced in order to enhance the torque-ripple measurement quality.

4.3 Comparison of the measured torque FRFs

An interesting property of the proposed excitation method is that the torque that is generated by the PMSM is known to a constant term (for an uncalibrated source) and therefore the direct current and/or torque to torque transfer function can be easily calculated. Figure 19 shows the calculated torque/current transfer function for testbench Nr. 1. & 2.

As we could see for the normalized tangential acceleration FRFs, that the most torque transfer is in the 500 – 1500 Hz band, however for testbench Nr. a 4th resonance is well visible above 2000 Hz. This peak can be also seen in the transfer functions of the normalized tangential acceleration, however not so clearly as in the torque/current FRF.

The coherence for the torque output is also worse compared to the coherence of the acceleration FRF, what can be explained by the low level of torque excitation and the low sensitivity of the torque sensor itself.

Nominally such an EPS PMSM roughly provides 5 Nm torque for 100 A peak phase current in all three phases, however in the FRF measurement 2 A peak current has been used only in one phase, which means roughly 0.1 Nm peak torque excitation maximum. The torque sensor provides 10 V output for 40 Nm DC torque, hence the output voltage was in the range of 25 mV peak, so 64 dB below the peak output and under such conditions the FRFs still show a useful 40 – 60 dB dynamic range and that is remarkable for such a test setup. Of course the resonances improve the Signal-to-noise ratio significantly, therefore in the actual measured torque may reach a few Newton meters during the periodic frequency sweep (Schröder multisine).

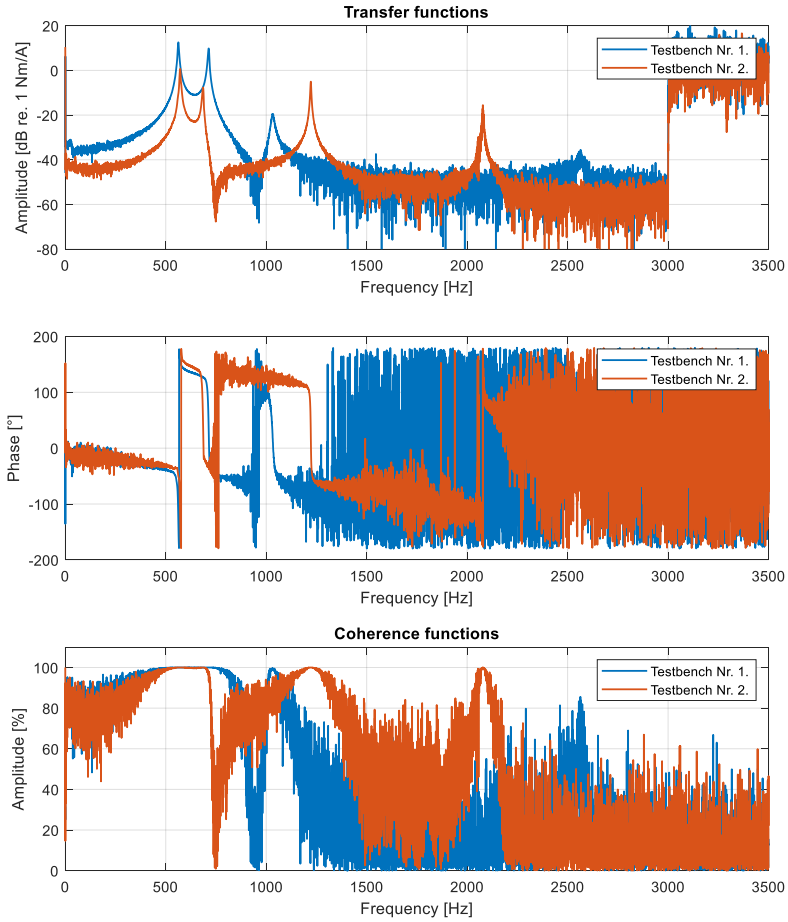

Figure 19: Measured FRFs and coherence functions between the excitation current and the torque sensor for testbench Nr. 1. (blue) & Nr. 2. (red).

5 Summary and conclusions

In this paper we propose a new torsional modal analysis method that does not require the investigated shaft system to rotate, but utilizes the attached Permanent Magnet Synchronous Motor as a torsional vibration exciter and therefore allows the angular acceleration to be measured using traditional accelerometers. The obtained transfer functions can be curve fitted using once again traditional modal parameter extractors, however a new 3D animation method is proposed to appropriately animate and hue torsional mode shapes thus enhance the understanding of torsional vibration phenomena.

After reviewing all the steps of the proposed method, the complete torsional modal analysis of two different PMSM testbenches are presented. First the mechanical setup is explained, which is followed by the measured FRFs and coherence functions, the results of the FRF estimation using Rational Fractional Polynomial method and the presentation of the obtained mode shapes. The results clearly show that the suggested torsional modal analysis method is applicable in practice and provides very good quality results for various test setups.

Furthermore it has been showed that the direct torque/current transfer function can be evaluated and analyzed, therefore the proposed excitation method opens up new ways for direct measurement of torque-ripple transfer in such a test setup and possibly in more complicated assemblies as well.

Acknowledgements

The author is truly grateful for many-many exceptional colleagues working at thyssenkrupp Components Technology Hungary Ltd. for the unwavering support in various filed of NVH activities. Special thanks to Mr. Kristóf Horváth who programmed the RFP algorithm for MIMO systems and provided his MATLAB implementation as well for the curve fittings in this investigation.

References

[1] T. Kimpián, Sz. Gungl, D. Pokol, T. Ungvári, Cs. Aranyi, "Vibro-Acoustic Simulation of Electric Motors in EPAS Systems", in *The 9th Congress of the Alps Adria Acoustics Association – Conference Proceedings*, 2021. September 23-24., pp. 154-159.

[2] O. Døssing, *Part II: Modal Analysis and Simulation*, Brüel and Kjær, March 1988

[3] C. Sihler, "A novel torsional exciter for modal vibration testing of large rotating machinery", *Mechanical Systems and Signal Processing*, Vol. 20, Feb. 2005, pp. 1725−1740.

[4] J. C. Wachel, F. R. Szenasi, "Analysis of torsional vibrations in rotating machinery", *Proceedings of 22nd Turbomachinery Symposium*, 1993, Texas, pp. 127-151.

[5] T. Kimpián, F. Augusztinovicz, "Torsional modal analysis of single shaft systems containing permanent magnet synchronous motors using novel broadband torque excitation method", *Proceedings of ISMA2012-USD2012, International Conference on Noise and Vibration Engineering*, September 17-19, 2012, Leuven, Belgium, pp. 2081-2089.

[6] T. Kimpián, F. Augusztinovicz, "Universal broadband torsional exciter from a permanent magnet synchronous motor", *Proceedings of ISMA2014-USD2014, International Conference on Noise and Vibration Engineering*, September 15-17., 2014, Leuven, Belgium, pp. 1101-1109.

[7] T. Kimpián, F. Augusztinovicz, "Multiphase multisine signals – Theory and practice", *Proceedings of ISMA2016-USD2016, International Conference on Noise and Vibration Engineering*, September 19-21., 2016., pp. 2041–2250.

[8] https://www.esi-audio.com/products/maya44usb+/

[9] https://www.lem.com/en/hx-05np

[10] R. Pintelon, J. Schoukens, *System Identification – A Frequency Domain Approach*, IEEE Press, The Institute of Electrical and Electronics Engineers, Inc. New York (2001), ISBN 0-7803-6000-1

[11] M. H. Richardson, D. L. Formenti, "Parameter estimation from frequency response measurements using rational fractional polynomials", *Proceedings of the 1st IMAC Conference*, Orlando, FL, November 1982

[12] M. H. Richardson, D. L. Formenti, "Global Curve Fitting of Frequency Response Measurements using the Rational Fraction Polynomial Method", *Proceedings of the 3rd IMAC Conference*, Orlando, FL, January 1985